Design and Trajectory Optimization of a Morphing Wing Aircraft

John P. Jasa *
University of Michigan, Ann Arbor, MI, USA

John T. Hwang †
NASA Glenn Research Center (Peerless Technologies Corp.) Cleveland, OH, USA

Joaquim R. R. A. Martins ‡
University of Michigan, Ann Arbor, MI, USA

Adding morphing wing technology to aircraft could drastically reduce the fuel burn required to complete a certain mission. This gain comes from the wing being able to adapt to become optimal for the desired flight condition. For maximal benefit, we must design the wing, morphing inputs, and mission trajectory simultaneously. In this work, we perform gradient-based aerostructural optimization for a morphing Common Research Model wing while optimizing its nominal design, morphing twist across its mission, and its altitude profile. Using a morphing optimization approach that simultaneously optimizes the mission and design, we find a 0.2 to 0.7% fuel burn decrease compared to a non-morphing design optimization, where the benefit increases with range. We also compare the fully coupled optimization approach with a surrogate-based approach to determine if we can simplify the optimization problem while still arriving at the optimal result. We find that the surrogate-based approach finds an optimum within 1.5% of the optimum obtained from the fully coupled approach and that the difference is smaller for smaller ranges.

I. Introduction

Wing morphing is not a new concept. The Wright Brothers utilized morphing wings to control their famous Wright Flyer in 1903. Early work on the subject back in the 1980s suggested applications in aerodynamics [1, 2], radar observability [1], and survivability [3]. Some modern work has focused on variable camber wings [2, 4, 5] and aerostructural optimization of morphing wing aircraft [6, 7, 8, 9, 10, 11]. Fundamentally wing morphing gives the wing designer more freedom by allowing the shape to change throughout the flight. However, the ability to alter the shape begs the question: what shape should it be?

Burdette et al. addressed this question using a traditional multipoint approach and showed that there was potential for 2.58% fuel burn savings over a typical mission when morphing was applied to the NASA Common Research Model (CRM) concept [9]. They formulated their multipoint optimization objective as the average fuel burn, computed using the Breguet range equation, over a 7-point stencil. The stencil was selected to be representative of the cruise conditions seen on a reference mission for the aircraft they considered. In their work, the aerostructural analysis was done using a coupled Reynolds-averaged Navier–Stokes (RANS) computational fluid dynamics (CFD) and finite elements analysis (FEA) model that was computationally expensive. Additionally, computing the objective and constraints required 9 calls to the high-fidelity models (7 point stencil for cruise performance, plus 2 load conditions). Burdette et al. later analyzed mission performance of a morphing wing aircraft by constructing a surrogate model based off high-fidelity

*Ph.D. Candidate, Department of Aerospace Engineering, AIAA Student Member
†Research Engineer (contractor at NASA GRC), AIAA Member
‡Professor, Department of Aerospace Engineering, AIAA Associate Fellow

aerostructural results [10]. The surrogate model was constructed prior to the optimization and provided aerostructural performance data for design points in the Mach-C_L space.

Here we will take a more direct route by fully coupling the trajectory analysis with the aerostructural analysis to capture the wing performance directly in the mission simulation. The most realistic and robust way to optimize an aircraft is to consider its performance along its entire mission trajectory, as shown in previous work [12, 13, 7, 14, 15]. By tightly coupling the morphing with the trajectory we are able to capture the optimal morphing schedule across the entire mission and better understand the technology's impact on actual performance. However this approach will require a much larger number of calls to the coupled aerostructural model than was needed in the multipoint approach.

Although previous work has optimized the morphing control inputs across a mission or the optimal trajectory, there has not been any study that has considered both together, to the best of the authors' knowledge. Using high-fidelity methods for aerostructural morphing wing and trajectory optimization is intractable because of the high computational cost to analyze the complex system. We must use lower-fidelity models or surrogate models to reduce the design space so we can find an optimal design in a suitable timeframe.

By optimizing with the design, mission, and morphing optimization in a fully coupled problem, we can consider path-dependent applications. For example, thermal constraints, control rate limits, and weather pattern constraints are all path-dependent effects that necessitate the fully coupled optimization approach presented here. Although we could set up a surrogate model to interpolate the aerodynamic data, that would presuppose that each design point is independent of the previous mission states, which is not true for path-dependent problems.

In this work we analyze and optimize the nominal design, morphing inputs, and altitude profile over the mission of the CRM-based configuration. To solve the coupled aerostructural system, we use a vortex lattice method (VLM) for the aerodynamic analysis and a 6-DOF FEA model. Additionally, we use a surrogate model for the propulsion analysis and a collocation-based approach for the coupled trajectory-propulsion system. Then we optimize the design and trajectory of an aircraft with a morphing wing and compare the performance against a conventional aircraft. We then compare the fully coupled optimization approach with the surrogate-based approach presented by Burdette et al. [10].

This paper has two aims. First, to quantify the added benefits of morphing technology by performing fully coupled mission-design-morphing optimizations. Second, to compare the fully coupled approach with a surrogate-based approach to see if we can reduce the computational cost while achieving close to the same optimal result.

II. Overview

Before we present the problem formulation and resulting contributions, we outline the computational tools and background theory used.

A. Aerostructural design tool

We can efficiently analyze the coupled aerostructural system using inexpensive physics-based models. VLM and 1-D FEA models can accurately capture the coupling between the aerodynamic and structural disciplines. A coupled 1-D VLM-FEA model enables optimization of the spanwise distributions of the aerodynamic twist, chord, and structural thickness. We have implemented this model in the OpenAeroStruct software package [16]. It is an open-source aerostructural optimization tool coupling an extended VLM model with FEA using 6-DOF spatial beam elements that support axial, bending, and torsional loads.

OpenAeroStruct is written entirely in Python and uses the OpenMDAO framework [17], a NASA-developed open-source software framework for multidisciplinary design optimization. OpenMDAO enables derivative computation for gradient-based optimization using the MAUD architecture [18], which unifies all methods for computing discrete derivatives [19]. Therefore, OpenAeroStruct can compute derivatives using the adjoint method, which is especially computationally efficient for problems with high numbers of design variables. Fully analytic derivatives are provided for each component in the aerostructural optimization problem.

Although OpenAeroStruct does not model some of the physics actually present in aerostructural wing design, it generally captures the same general trends as high-fidelity methods. For example, compressibility effects, wave drag, and flow separation are not directly modeled, but we use empirical corrections to account for the absence of these effects. The structural system is modeled as an equivalent representative circular spar, which simplifies the moments

of inertia about the elastic axis as radially symmetric. OpenAeroStruct's relatively low cost allows us to use it in this fully coupled optimization while providing adequate resolution of the physics of the system.

B. Selection of morphing type

Wing morphing allows a single aircraft to perform optimally in different scenarios. The term "morphing" is used to describe vehicle adaptability of many types, including conformal control surfaces and camber variations, but also large changes in span, wing area, chord, etc [20]. The benefits of many different types of wing morphing have been studied in detail through simulations, wind tunnel, prototypes, and full-scale aircraft [21, 22]. To justify adding morphing technology to an aircraft, a designer must consider if the performance benefits outweigh the increased weight, system complexity, and program costs. Specifically, some engineering challenges that must be addressed are distributed high-power density actuation concepts, structural mechanization concepts, and flexible skins [20].

We examine twist morphing, where the aerodynamic twist at sections along the span can vary during flight while the airfoil profile remains unchanged. Twist morphing can be achieved by servos, shape memory actuators, piezoelectric actuators, or hydraulic actuators [22]. Depending on how the aircraft is configured, the twist morphing capability can have a minimal impact on the internal structural components of the wing. For example, if the main structural spar in the wing is at the quarter-chord and has a circular cross-section, the wing twist can more simply be actuated around this spar. Vos et al. achieved twist morphing in a prototype wing using threaded rods to independently rotate four ribs around a circular main spar [23]. Twist morphing is primarily examined for use in micro-air and small-scale vehicles, though it could be used in any scale of aircraft.

C. Context for mission optimization

Our mission optimization is motivated by work from Hendricks et al. [24] and Falck et al. [25] that coupled mission optimization with propulsion analysis and thermal constraints. Their work showed that by using a higher-order collocation method with gradient-based optimization and analytic derivatives, fully coupled mission problems are tractable. Falck et al. specifically examined how path-dependent thermal constraints affect the optimal mission profile of an electric aircraft, an application case that necessitates the use of fully coupled mission and design optimization [25]. Although individual disciplinary analyses could be performed to evaluate the aircraft performance, a fully coupled model more accurately resolves the interdisciplinary trade-offs between the thermal constraints and heat generation.

Other work has focused on using surrogate models to feed aerodynamic performance information to the mission optimization problem. Kao et al. used a surrogate model with training data points generated by a panel code [15] for a fixed design. Hwang and Martins used a surrogate model trained with data obtained by solving the Euler equations for each design in the optimization loop [13]. They also optimized the design of the wing while optimizing the mission profile. Burdette et al. considered morphing performance over a fixed mission using a pre-trained surrogate with optimized morphing inputs [10]. They created the surrogate using training points from the Mach-C_L space based on where the aircraft would fly during the fixed mission. The resulting surrogate model was then used in the mission analysis to find the optimal aerodynamic performance of the morphing wing at each queried flight condition.

This naturally raises the question: do we need to explicitly evaluate the aerostructural performance within the mission analysis in a fully coupled manner, or can we use surrogate models and obtain reasonably accurate results? For applications and missions that are not path-dependent, we could expect that the surrogate models could reasonably resolve the design-mission trade-offs with reduced computational expense. However, these surrogate models are trained with data that does not consider the aircraft's previous state in the mission profile. Because of this, the surrogate-based approach cannot accurately resolve path-dependent effects like thermal constraints, actuator motion limits, or discontinuous aircraft weight resulting for ordinance delivery, for example. These applications require the fully coupled design-mission approach presented in this paper.

D. Common Research Model background

As an application case we use a wing model based on the undeformed Common Research Model (uCRM) [26], a large-scale transport aircraft wing developed by the MDOlab at University of Michigan. Figure 1 shows the Boeing 777 wing-body next to the uCRM wing-body. The uCRM is based off the CRM developed by Vassberg et al [27]. Brooks et al. adapted the CRM into the uCRM for use in aerostructural analyses and optimizations [26]. They did this

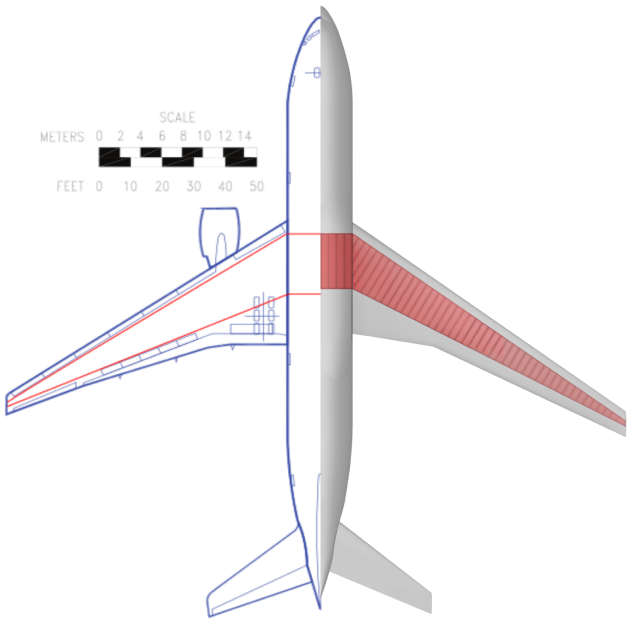

Figure 1. Boeing 777 (left) and uCRM-9 (right). The uCRM has a slightly lower wing area and span, and more sweep than the Boeing 777 [26].

by back-calculating the jig shape of the CRM wing and producing an aerostructural model. For this paper, we take the baseline CRM geometry and remove the vertical displacements to create a low-fidelity geometry that is close to the uCRM definition.

The CRM was originally developed as a benchmark configuration for aerodynamic analysis to validate CFD. It has been used extensively to compare simulation methods against each other and against wind tunnel tests [28]. The CRM model is also used in the Drag Prediction Workshop, where multiple institutions and companies run the same analysis cases to compare results from different CFD solvers. Because of this, a large trove of information is available on the performance of the CRM, which makes it an excellent candidate for investigating new analysis and optimization methods. We are using this model because it is well-studied and we understand how the wing behaves at many flight conditions.

III. Methodology

In this section, we describe the methods and algorithms in the multidisciplinary model that incorporates mission analysis, aerostructural analysis, and a propulsion surrogate model. We discretize the mission profile, enforcing the horizontal and vertical equations of motion and integrating an ordinary differential equation (ODE) to solve for the fuel burn profile. At each mission point, the aerodynamic and structural responses are computed, and the propulsion characteristics are predicted using a surrogate model. In the subsections that follow, we describe the mission equations, the integration of the resulting ODE, and the solution algorithm for the coupled system.

A. Governing equations for mission analysis

The aircraft equations of motion are

$$T\cos\alpha - D - W\sin\gamma - m\dot{v}_y\sin\gamma - m\dot{v}_x\cos\gamma = 0, \tag{1}$$

$$L + T\sin\alpha + m\dot{v}_x\sin\gamma - W\cos\gamma - m\dot{v}_y\cos\gamma = 0, \tag{2}$$

where L, D, T, and W are the forces of lift, drag, thrust, and weight, m is the mass of the aircraft, $\dot{v}_x$ and $\dot{v}_y$ are the acceleration components, γ is the climb angle, and α is the angle of attack. These two equations are in the horizontal and vertical directions, respectively, with respect to the flow velocity. The equations of motion are discretized and enforced at each resulting point. The third governing equation is the ODE for fuel weight,

$$\dot{W}_f = T \cdot SFC \tag{3}$$

where W_f is the fuel weight and SFC is thrust-specific fuel consumption. Both thrust and SFC are functions of W_f. We describe the integration of this ODE in more detail in the next sub-section.

B. ODE Integration

Because of the fuel burn equation, the governing equations for the mission analysis can be viewed as an ODE with many constituent parts. We can either view and solve the mission equations with the two equations of motion and the fuel burn equation treated separately, or as a single ODE with the two equations of motion embedded in the right-hand side of the ODE function. We choose the former approach for modularity.

Regardless of the approach, we must integrate an ODE and compute the derivatives of the integration, i.e., the derivatives of the integrated ODE state variables with respect to the inputs to the ODE. For this, we use Ozone [29], an ODE solver library for OpenMDAO with several unique characteristics. Ozone uses the general linear methods formulation, which unifies all linear multi-step and Runge–Kutta methods, allowing any specific method to be implemented by simply specifying 4 matrices of coefficients. Therefore, Ozone has roughly 50 integration methods implemented, and all are differentiated so that they can be used in an adjoint-based optimization approach.

Ozone also provides the choice of 3 approaches: time-marching, solver-based (where the ODE states are computed by solving a nonlinear system), and optimizer-based (where the ODE states are turned into design variables with associated constraints). A benchmarking study found that the solver-based approach is the most computationally efficient and that Gauss–Legendre collocation provides the best combination of accuracy and computation time among integration methods [29]. The solver-based approach is more efficient than time-marching because of the overhead due to OpenMDAO when sequentially evaluating at time steps. The solver-based approach allows for vectorization of the aerostructural analyses, i.e., the VLM and FEA models, across the nodes in the mission analysis. Therefore, we use the solver-based approach with 6th-order Gauss–Legendre.

C. Coupled solution

The mission equations have a coupling loop, as we can see in a model visualization in Fig. 2. The figure shows the hierarchy tree for the model and the dependency graph for the constituent components and variables. The ‘sys_coupled_analysis‘ group contains the coupling loop: the vertical equation of motion computes lift from weight, the OpenAeroStruct group computes drag from lift, the horizontal equation of motion computes thrust from drag, then we compute throttle from thrust, then thrust-specific fuel consumption from throttle, and finally we integrate the fuel burn ODE. The integration produces fuel weight, from which we obtain the total aircraft weight, and the loop closes.

As shown in Fig. 3, the mission analysis contains a coupling loop (at the ‘sys_coupled_analysis‘ level), but the ODE solver itself also contains a coupled system of equations (at the ‘fuel_rate_ode‘ level). The latter coupling is present because we use the solver-based formulation in Ozone for fast vectorization. Instead of using nonlinear solvers at both levels, we find it more efficient in numerical experiments to apply a single nonlinear solver—the nonlinear block Gauss–Seidel algorithm—at the top level. Typically, the nonlinear system at the ‘sys_coupled_analysis‘ level converges in 10-20 iterations.

The aerostructural analysis using the VLM and FEA methods is one of the blocks in the coupling loop in ‘sys_coupled_analysis‘. We can view this block as a mapping from lift to drag; however, the aerostructural model computes both lift and drag as outputs as a function of angle of attack. Since robustness and efficiency are both required, we use a bracketed root finding algorithm. A bracket is almost always successfully found by choosing a large negative and a large positive angle of attack since we do not model stall.

The propulsion surrogate model uses the regularized minimal-energy tensor-product spline interpolant [30]. The inputs are throttle setting, Mach number, and altitude, and the outputs are thrust and thrust-specific fuel consumption. The data is generated from the Numerical Propulsion System Simulation (NPSS) software [31] for a Boeing 777-sized

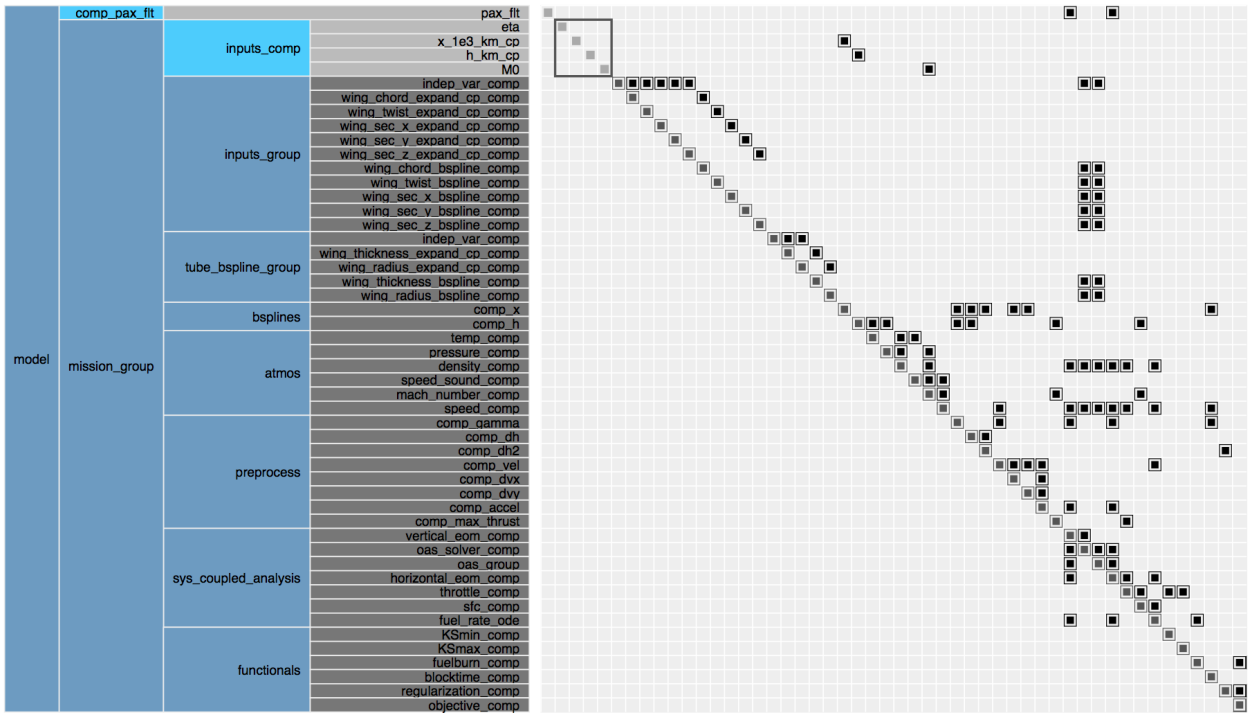

Figure 2. Hierarchy tree and dependency graph for the overall model.

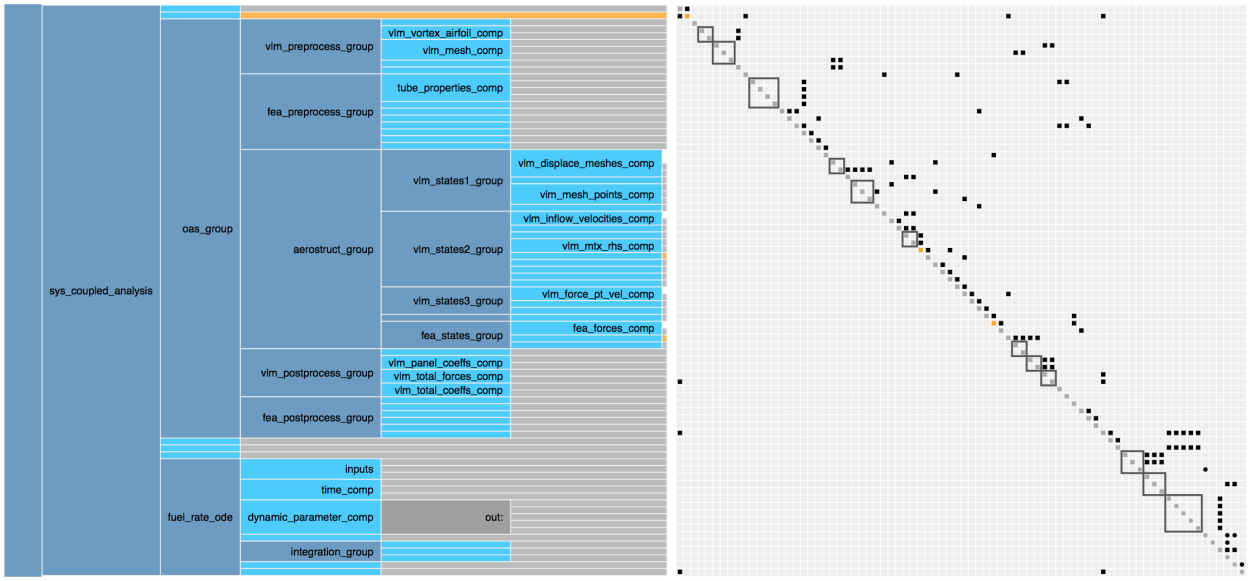

Figure 3. Hierarchy tree and dependency graph, zoomed in on the mission sub-model which contains the aerostructural analysis.

engine. Thrust is linear in throttle setting, so the throttle is computed in 'throttle_comp' by evaluating the maximum thrust for the Mach number and altitude of interest and normalizing the current thrust by the maximum thrust.

IV. Problem formulation

In this section, we describe the 4 types of optimization problems that we solve in this paper: fixed-design, static-design, direct morphing, and surrogate-based morphing. The objective function, design variables, and constraint functions for each problem are presented in Table 1. Fixed-design optimization is the baseline problem where only the mission is optimized, and static-design optimization optimizes the mission and the wing design without considering morphing. The direct morphing optimization and surrogate-based morphing optimization simultaneously optimize the mission and the morphed design at each point, but they consider morphing in different ways. In all 4 cases, the objective function is fuel burn over the entire mission.

Table 1. Optimization problem formulations for each of the three cases.

Category	Name	Quantity				Lower	Upper	Units
		Fixed-design	Static-design	Direct morphing	Surrogate-based morphing			
Objective	fuel burn	1	1	1	1	–	–	kg
Variables	twist	0	5	125	0	–3	8	degrees
	spar thickness	0	5	5	0	0.01	0.5	m
	altitude profile	25	25	25	25	0	14	km
	Total	**25**	**35**	**155**	**25**			
Constraints	von Mises (KS)	0	1	1	0	0	$\frac{\sigma_{yield}}{2.5}$	Pa
	min. slope	25	25	25	25	–20	20	degrees
	max. slope	25	25	25	25	–20	20	degrees
	min. thrust (KS)	1	1	1	1	0.01		
	max. thrust (KS)	1	1	1	1		1.00	
	Total	**52**	**53**	**53**	**52**			

In all design and morphing optimizations, the wing twist and thickness profiles are optimized using B-splines where the design variables are the B-spline control points. The aerostructural model used in OpenAeroStruct is shown in Figure 4. The vortex-lattice and finite-element meshes for the wing have 19 span-wise nodes and 5 span-wise control points. The mission profiles are discretized with 25 nodes in all cases. The initial twist and thickness distributions for all optimizations were determined using a 5-point multipoint optimization with 5 different cruise conditions. This ensures that the fixed-design optimization has near-optimal twist and thickness distributions as opposed to the baseline design. We use a sequential quadratic programming algorithm called Sparse Nonlinear OPTimizer (SNOPT) [32] as the optimizer for these problems.

We now discuss each of the 4 types of optimization problems in more detail.

A. Fixed-design optimization

The first optimization problem is a mission-only optimization that provides a baseline for evaluating the impact of static-design optimization on fuel burn. The design variables are the altitude values at the 25 mission points, as we see in Table 1. Minimum and maximum slope constraints are enforced at each mission point; these are linear constraints that improve robustness of the optimization by eliminating unreasonable altitude profiles. Minimum and maximum thrust constraints are also enforced since thrust profile is an output of the model given altitude profile is an input. Since these are nonlinear constraints, they are aggregated using Kreisselmeier–Steinhauser functionals [33] for more efficient derivative computation. These mission-related design variables and constraints are included in the other three optimization problems as well.

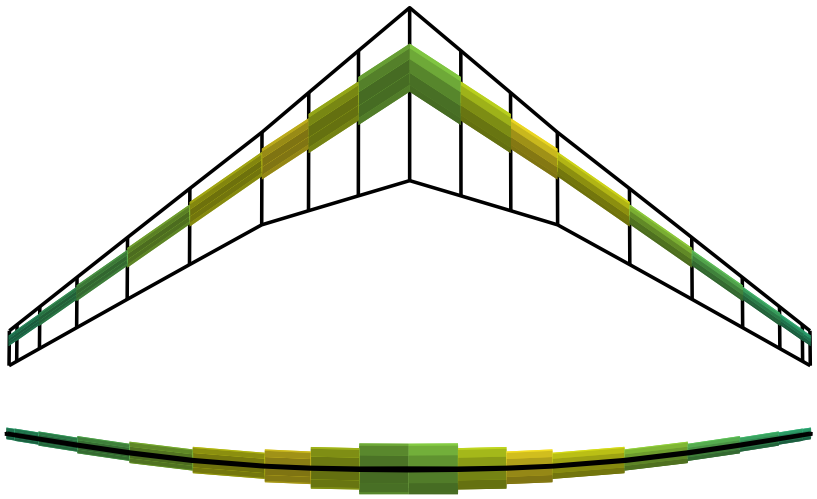

Figure 4. Top and front view of the multipoint optimized wing from OpenAeroStruct showing the structural spar and the lifting surface mesh.

B. Static-design optimization

The second optimization problem includes the mission-related design variables and constraints and adds the wing design without morphing to the problem. As we see in Table 1, the twist and structural thickness parameters are now design variables, but these values are static throughout the mission. Therefore, this is a simultaneous mission-design optimization that designs the optimal wing with no morphing capability. Since the structural thickness parameters are optimized, we enforce von Mises stress constraints, aggregated using Kreisselmeier–Steinhauser functionals [33] as we did with the thrust constraints.

C. Direct morphing optimization

The third optimization problem now adds morphing to the previous problem. The only difference from the static-design optimization is that the twist distribution is not static over the mission, but allowed to take on different values at each mission point. As we see in Table 1, this is the largest optimization problem because the twist is discretized both span-wise and over the mission profile. We call this the 'direct' morphing optimization problem because the final problem uses an indirect approach to capturing morphing that is cheaper, but introduces some error.

D. Surrogate-based morphing optimization

The final optimization problem also considers morphing, but using a different approach. It is significantly different from the other three formulations because OpenAeroStruct is not directly evaluated during the optimization. Instead, 400 aerostructural optimizations are performed offline using OpenAeroStruct to train a surrogate model that is evaluated during the actual optimization.

The 2D surrogate model uses the regularized minimal-energy tensor-product spline (RMTS) interpolant [30]. The inputs of this surrogate model are lift coefficient and dynamic pressure, and the outputs are drag coefficient and angle of attack for the twist distribution-optimized wing for the given, desired lift coefficient and dynamic pressure. Building and using this surrogate model allows the higher-level mission-morphing optimization to cheaply get an estimate of the best possible drag coefficient for each given lift coefficient, assuming the wing is morphed to the optimal twist distribution at that lift coefficient.

We highlight two characteristics of this approach. First, it is an alternative to the direct morphing optimization that is much cheaper because a surrogate model is evaluated when converging the mission equations, rather than OpenAeroStruct itself, and the 125 twist design variables are not included in the optimization problem because they are pre-optimized in the training data. Second, it is an approximation with error due to the surrogate model, and

due to assuming a conservative thickness distribution. While pre-computing the optimal twist distributions for given lift coefficients is efficient, it requires assuming a structural thickness distribution. We do not know this distribution *a priori*, so we must be conservative to ensure that the surrogate-based morphing optimization does not use a lift coefficient profile for which the failure limits are exceeded for a subset of the points.

V. Quantifying the benefits of morphing

Here, we solve the first three optimization problems described in Table 1 (leaving out the surrogate-based morphing optimization) with three mission ranges—1000 nm, 3000 nm, and 7000 nm. The resulting optimal fuel burn values are shown in Table 2 and plotted in Fig. 5 as normalized fuel burn values with the fixed-design mission optimization result as the reference. For each of the three mission ranges, the morphing wing outperforms the static-design as expected. Compared to the static-design, the morphing wing sees between 0.2 to 0.7% fuel burn improvement, with the long range mission seeing the biggest improvement. The fixed-design approach has a set thickness distribution which is overly conservative for the short and medium range missions, but is closer to the optimal thickness distribution for the long range mission. This is why we see the fixed-design for the long-range mission yield a fuel burn value closer to the static-design and direct morphing cases. For different aircraft with more varied mission profiles, we would expect to see a larger increase in performance from the addition of morphing technology.

Table 2. The morphing wing always has a lower fuel burn value than either other case, as expected. The benefits of morphing technology are more pronounced in the long range mission where the fuel burn benefit from lower structural weight is larger.

	Fuel burn, kg		
	1000 nm	3000 nm	7000 nm
fixed-design	14 697.7	41 879.9	116 774.0
static-design	14 215.4	40 228.5	114 613.0
Morphing design	14 181.9	40 053.3	113 848.8

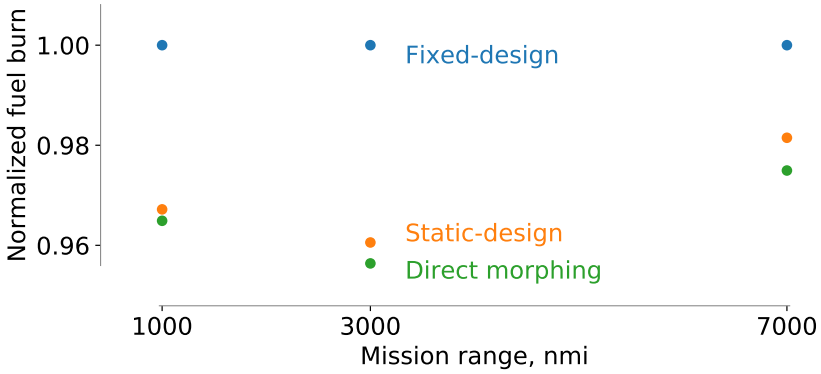

Figure 5. The relative decrease in fuel burn obtained with morphing technology varies based on the mission range. The long range mission using direct morphing sees the biggest improvement in fuel burn compared to the static-design.

We now investigate the results from the 1000 nmi and 7000 nmi missions in more detail, in Fig. 6 and Fig. 7 respectively. Figure 6 shows more information from the short-range optimizations for the fixed-design, static-design, and morphing cases. Here we see that the morphing wing uses slightly less fuel for the entire mission, but all of the resulting curves are very close to the results from the static-design. The altitude profile is limited by the upper bound of 14 km during the cruise segment. For this short mission, the fuel weight and thus the aircraft weight are relatively low, which means that the optimal flight altitude is higher than that for a heavier aircraft. This altitude limit forces the aircraft to fly at a suboptimal L/D ratio, which we see during the cruise segment of the mission. We would expect to see a greater benefit from morphing technology if we included operational constraints, such as constant flight

level cruise segments. This would force the aircraft to fly at more distinct flight conditions, which would cause the static-design to be less optimal over the entire mission.

Each optimization method yields roughly the same altitude, path angle, and velocity profile, but the largest differences are seen in the C_L and L/D profiles. The fixed-design case is forced to optimize the mission with a fixed structural weight for a conservative structure, which forces it to fly at a slightly higher C_L. For this optimization case and others, we see that the L/D ratio is higher than expected. We use C_L and C_D offsets to account for the lift at zero angle of attack and the drag components from the rest of the aircraft; however, we suspect that the drag is underpredicted, which is the cause of the relatively high L/D values we see.

Figure 7 shows results from the long range mission using the same three optimization formulations. As expected, the altitude increases and the angle of attack decreases as fuel is burned, since the aircraft can sustain level flight with less total lift. Thrust slightly decreases throughout the cruise segment, and L/D improves throughout the mission as the aircraft can fly at a more optimal flight condition. Additionally, the fixed-design optimization requires a higher C_L at the beginning of the mission due to its aerodynamic inefficiency. This also leads to the increased thrust for the fixed-design optimization. Near the end of the mission profiles, we see jagged jumps in the C_L and L/D profiles, especially for the fixed-design case. We believe this result is due to numerical effects, such as the relatively coarse mission discretization or noise in the function evaluation, and they merit further investigation.

VI. Direct morphing approach compared to the surrogate-based morphing approach

We now compare the results from the direct morphing optimization to those from the surrogate-based optimization. One main difference between these two formulations is that the direct morphing optimization has the ability to tailor the structural thickness and the morphing inputs simultaneously, which produces a more efficient structural thickness distribution. This allows for a decrease in fuel burn compared to the relatively conservative approximation of the internal structure for the surrogate-based method. On the other hand, the surrogate-based optimization is much less computationally expensive because we do not have to repeatedly solve the coupled aerostructural system during the optimization.

To compare these two methods, we select an optimized surrogate based on a quasi-optimal structural thickness distribution that does not allow the spar to fail during the mission. We do this by creating multiple surrogates with different multiplicative factors on the baseline structural thickness to see what the minimum factor is that avoids structural failure. We use the baseline thickness distribution as determined previously by the 5-point multipoint optimization and multiply by a thickness factor to obtain the new structural thickness distribution. We then optimize the morphing inputs at 400 design points and construct a surrogate model for each thickness factor as described in Sec. IV D. With a set of surrogates, we can now perform relatively inexpensive mission optimizations and determine which factor produces the lowest fuel burn while not allowing the spar to fail.

Figure 8 shows the structural failure values throughout the missions for mission optimizations with thickness factors ranging from 1.0 to 2.0 in increments of 0.1. The failure constraint is the calculated KS function for the entire spar, where if the value is above 0, the von Mises stress has exceeded the yield stress, causing structural failure. We see that the failure constraint value decreases over the mission in each case as the aircraft burns fuel and becomes lighter, which in turn lowers the aerodynamic loads acting on the wings. For the thickness factor values below 1.4, the structural spar fails near the beginning of the mission. Therefore, 1.4 is the minimum structural spar thickness factor to avoid failure during the limiting load case, which is climbing during the long range mission. A more conservative thickness factor could be used to account for load cases not explicitly considered here, like a 2.5g pull-up maneuver. A plot such as Figure 8 can help a designer understand how conservative of a structural model to use when constructing the morphing-optimized surrogate.

For the short and the medium range mission, a thickness factor of 1.0 can be used without the spar failing. This is because in both cases, the plane is lighter because it needs less fuel to complete the mission. This means that the aerodynamic loads are less than those from the long range mission. For each comparison going forward, we use a thickness factor of 1.0 for the short and medium range missions and 1.4 for the long range mission. Each of the short, medium, and long range optimizations are performed independently of each other and do not depend on results from other mission lengths, which allows us to use different thickness factors. This is consistent with the direct morphing approach, where each mission range was independent of each other as well, which means that each optimized design could have a different thickness distribution.

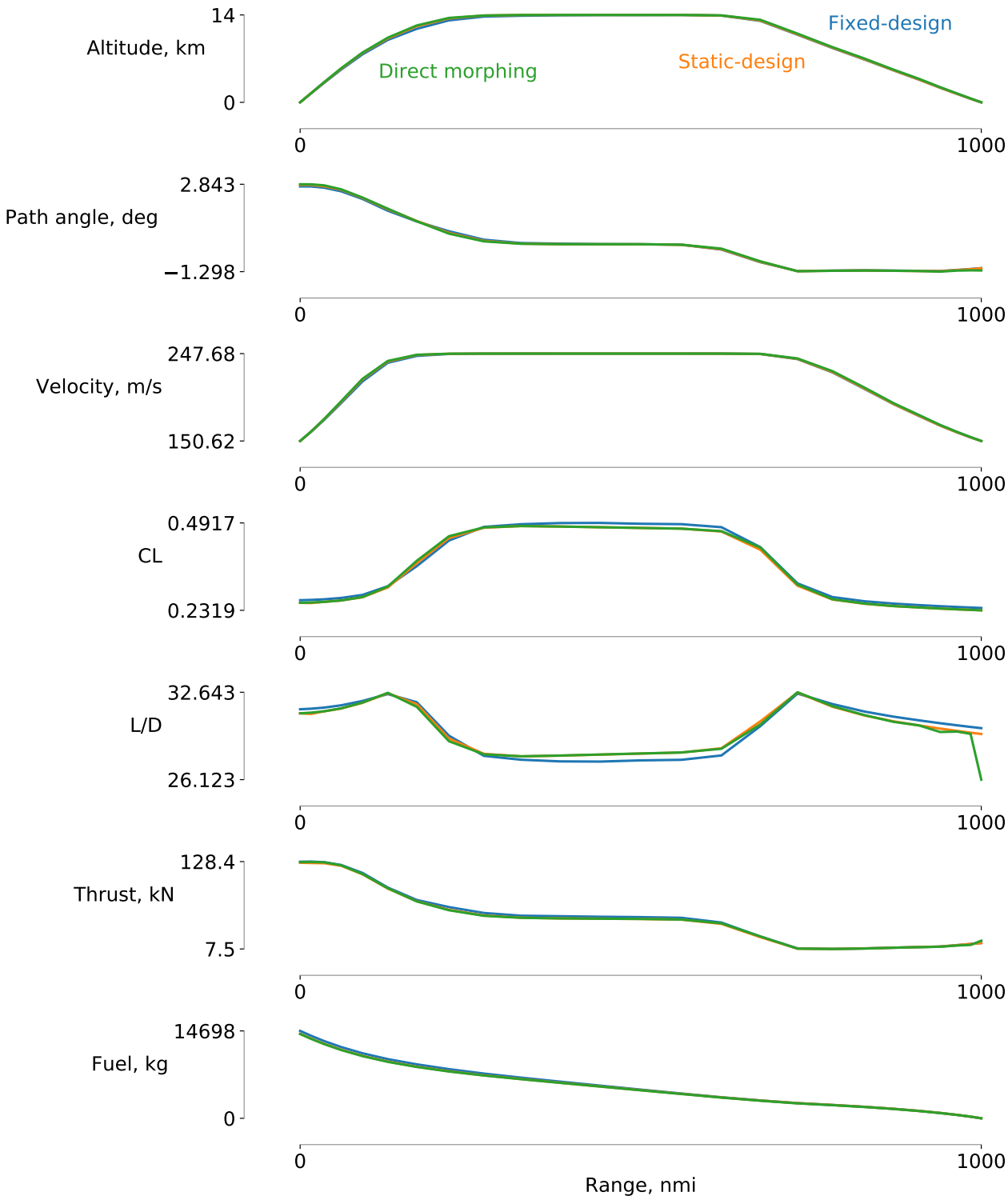

Figure 6. Each of the optimization methods yields aerodynamic and mission profiles that are similar. The main differences come from the higher C_L seen for the fixed-design case, where the relatively inefficient design necessitates a larger amount of lift.

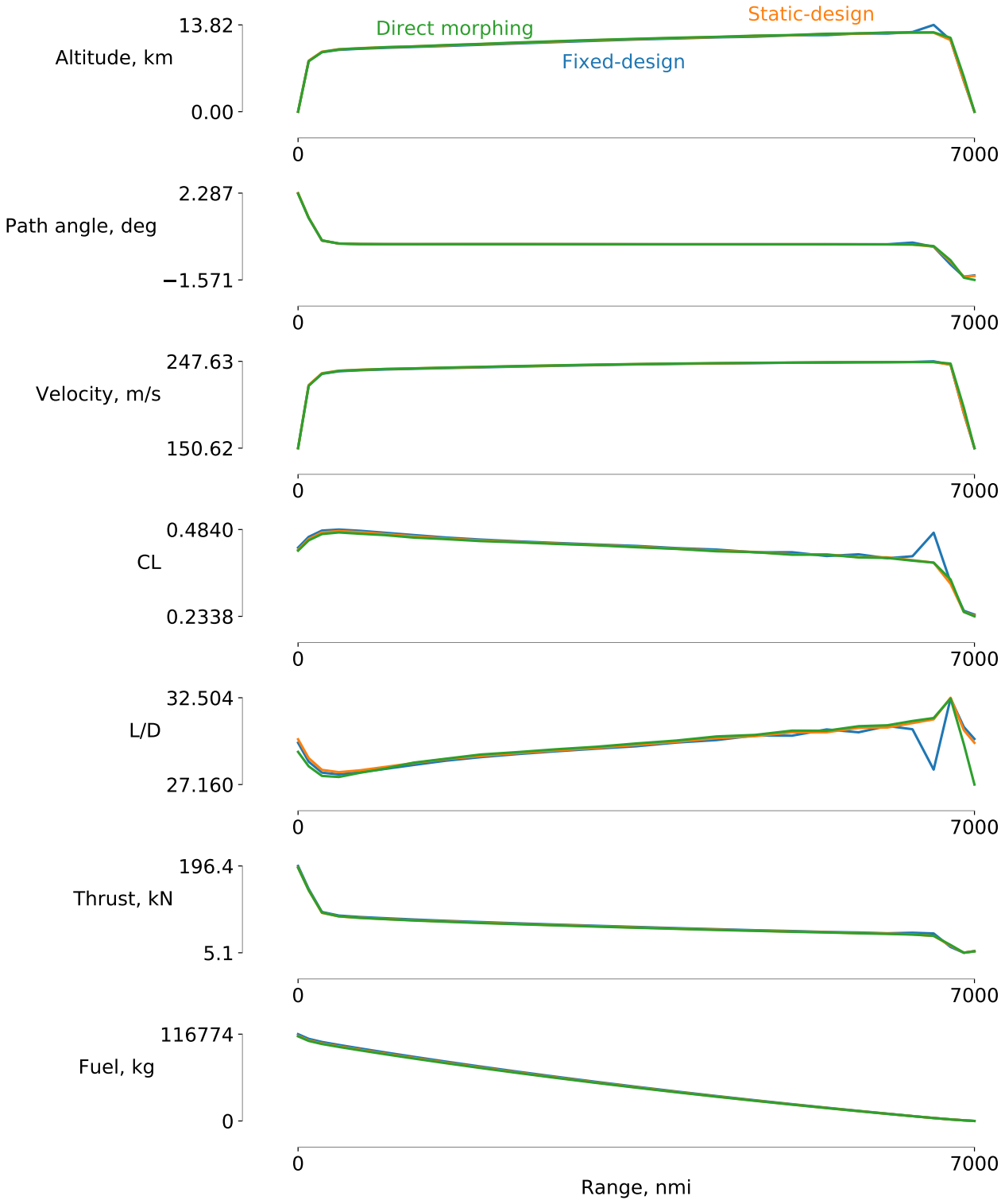

Figure 7. Most of the gains of morphing technology come from tailoring the structural properties of the wing to achieve a minimal spar weight while avoiding structural failure. The lighter weight aircraft can fly at a slightly lower C_L which produces a lower fuel burn. Near the end of the mission profiles, we see sharp changes in the C_L and L/D, especially for the fixed-design case. These rapid changes need to be investigated in more detail to see if they are a result of numerical noise or some other effect.

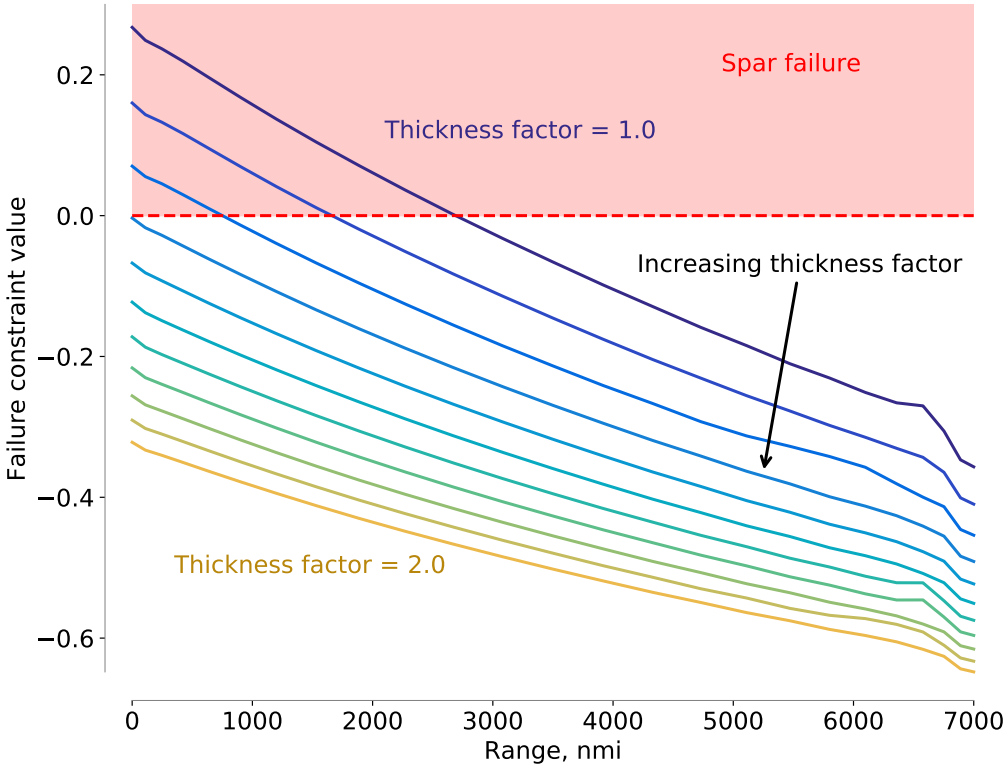

Figure 8. A thickness factor of 1.4 avoids structural failure on the long range mission, which is the limiting case for structural loads. The spar failure region is at the beginning of the long range mission, where the aircraft is the heaviest.

With the minimum thickness factor needed in each case to avoid failure, we can now compare the results from the surrogate-based optimization with the direct morphing optimization. Figure 9 shows the normalized fuel burns for all three mission ranges for both methods. The short range missions sees a fuel burn improvement of 0.4% whereas the long range mission sees an improvement of 1.5% when using the direct morphing approach. We see a decrease in fuel burn using the direct morphing approach because the optimizer can exploit the ability to tailor the structural thickness for the limiting case based on the aerodynamic loads. Additionally, the reduced structural weight has a larger impact on the fuel burn over the long range mission due to the corresponding reduced fuel weight required to complete the mission.

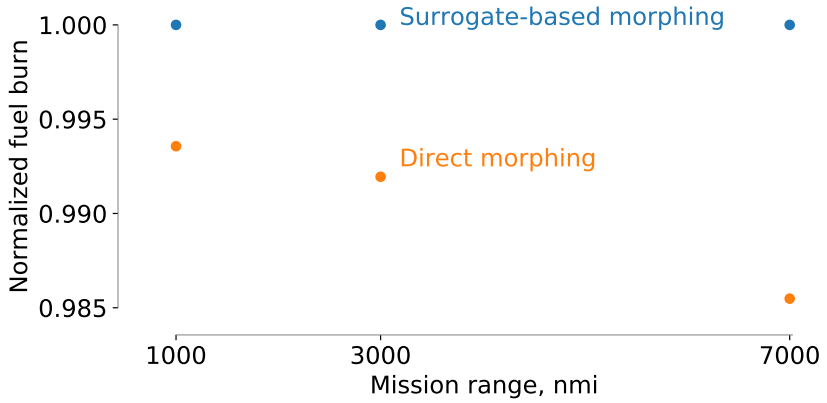

Figure 9. The direct morphing approach yields the biggest gains in the long range mission, where we see a 1.5% decrease in fuel burn. This effect is mostly due to the direct morphing optimization being able to tailor the structural thickness distribution and the morphing twist simultaneously to find the optimal balance between load alleviation, weight, and aerodynamic performance.

Next, we compare some of the aerodynamic and mission parameters for surrogate-based and direct morphing approaches over the long range mission. Figure 10 shows that the surrogate model approximates the aerodynamic properties of the direct morphing problem very accurately. Both optimizations converge to essentially the same altitude, path angle, velocity, and thrust profiles. We can see slight differences between the optimized results for the two methods in the C_L and L/D plots where it appears that the surrogate model has some amount of oscillations or noise near the end of the mission. This might be due to the relatively coarse mission discretization of 25 collocation nodes or modeling error from the surrogate model, though further investigation is required. Because the aerodynamic and mission properties are close to the same in both cases, this suggests that the majority of the decrease in the fuel burn comes from the difference in thickness distributions.

VII. Conclusion

To design a morphing wing aircraft for optimal performance, we must optimize its nominal design, mission profile, and morphing inputs in a tightly coupled problem. Explicitly simulating the aircraft's aerostructural response at each flight condition in the mission allows us to directly quantify the benefits of the design obtained from performing this direct morphing optimization. We make this problem tractable by using low-fidelity physics-based models, a high-order collocation method for the mission analysis, analytic derivatives for every component in the problem, and gradient-based optimization to quickly reach the design optimum. With this framework set up, we can also optimize aircraft designs while considering path-dependent effects.

We used this direct morphing formulation to compare optimization results for a morphing wing to a static-design wing for a commercial airliner. The direct morphing result achieved a 0.2 to 0.7% fuel burn reduction compared to the static-design optimized result, where the reduction is larger for longer missions. As expected, the performance gains from adding morphing technology to a commercial airliner wing are very small. Using this direct morphing approach to evaluate the gains from morphing technology for other aircraft with more complex missions or more articulate morphing mechanisms would result in a larger increase in performance.

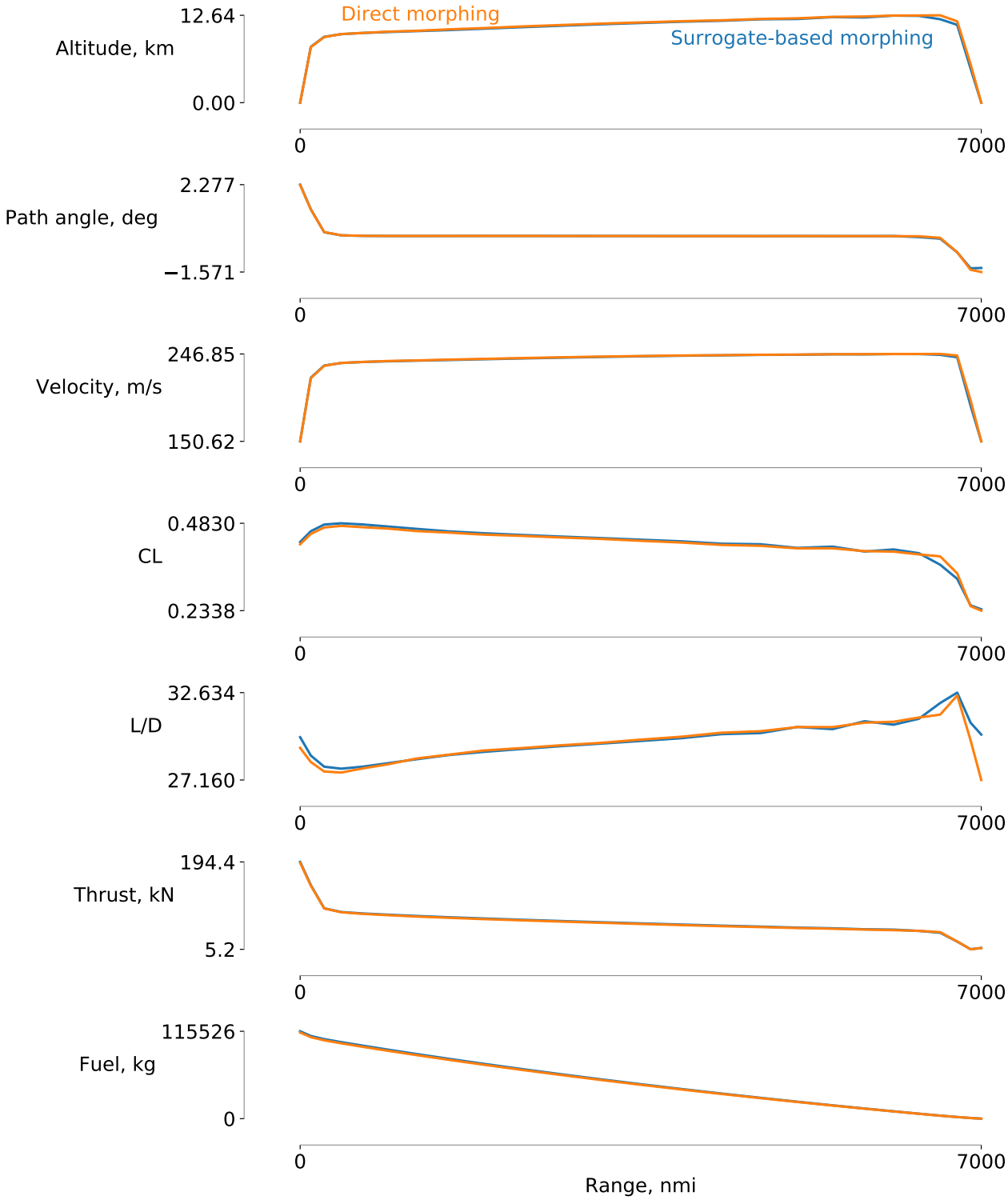

Figure 10. The aerodynamic properties of the direct morphing optimization compared to the surrogate-based optimization are extremely similar. This suggests that the main difference in fuel burn comes from the ability to decrease the aircraft weight through tailoring the structural thickness distribution.

We also compared the direct morphing method with a surrogate-based morphing method to evaluate the extent that the problem can be simplified using a surrogate model. We found that the surrogate-based morphing approach can find an optimum within 1.5% of the optimum obtained from the direct morphing method. This percentage difference is greater than the gain seen from using the direct morphing approach compared to the static-design. The direct morphing method was able to correctly resolve the aerostructural-morphing trade-offs in a way that the surrogate-based morphing approach could not. If there is not a strong coupling between aerodynamics, structures, and propulsion, the surrogate-based approach may be suitable. For highly coupled systems or path-dependent optimization problems, the fully coupled optimization approach is required.

VIII. Acknowledgements

The first author is grateful for support from the National Science Foundation Graduate Research Fellowship under Grant No. DGE-1256260. The second author was supported by the NASA ARMD Transformational Tools and Technologies Project. The authors thank Justin Gray for fruitful discussions on how to reformulate OpenAeroStruct and approach the coupled problem.

References

[1] Gilbert, W. W., "Mission adaptive wing system for tactical aircraft," *Journal of Aircraft*, Vol. 18, No. 7, 1981, pp. 597–602.

[2] Szodruch, J. and Hilbig, R., "Variable Wing Camber for Transport Aircraft," *Progress in Aerospace Sciences*, Vol. 25, 1998, pp. 297–328.

[3] Bonnema, K. and Smith, S., "AFTI/F-111 mission adaptive wing flight research program," *4th Flight Test Conference*, 1988, p. 2118.

[4] Bolonkin, A. and Gilyard, G. B., "Estimated benefits of variable-geometry wing camber control for transport aircraft," 1999.

[5] Kota, S., Hetrick, J., Osborn, R., Paul, D., Pendleton, E., Flick, P., and Tilmann, C., "Design and Application of Compliant Mechanisms for Morphing Aircraft Structures," *Proceedings of the SPIE Smart Structures and Materials Conference*, San Diego, CA, March 2003.

[6] Gamboa, P., Vale, J., P. Lau, F., and Suleman, A., "Optimization of a morphing wing based on coupled aerodynamic and structural constraints," *AIAA journal*, Vol. 47, No. 9, 2009, pp. 2087–2104.

[7] Molinari, G., Quack, M., Dmitriev, V., Morari, M., Jenny, P., and Ermanni, P., "Aero-Structural Optimization of Morphing Airfoils for Adaptive Wings," *Journal of Intelligent Material Systems and Structures*, Vol. 22, No. 10, 2011, pp. 1075–1089. doi:10.1177/1045389X11414089.

[8] Fujiwara, G. E. and Nguyen, N. T., "Aerostructural Design Optimization of a Subsonic Wing with Continuous Morphing Trailing Edge," *35th AIAA Applied Aerodynamics Conference*, 2017, p. 4218.

[9] Burdette, D. A., Kenway, G. K., and Martins, J. R. R. A., "Performance Evaluation of a Morphing Trailing Edge Using Multipoint Aerostructural Design Optimization," *57th AIAA Structures, Structural Dynamics, and Materials Conference*, AIAA, January 2016. doi:10.2514/6.2016-0159.

[10] Burdette, D. A., Kenway, G. K. W., and Martins, J. R. R. A., "Aerostructural design optimization of a continuous morphing trailing edge aircraft for improved mission performance," *17th AIAA/ISSMO Multidisciplinary Analysis and Optimization Conference*, June 2016. doi:10.2514/6.2016-3209.

[11] Burdette, D., Kenway, G. K. W., Lyu, Z., and Martins, J. R. R. A., "Aerostructural Design Optimization of an Adaptive Morphing Trailing Edge Wing," *Proceedings of the AIAA Science and Technology Forum and Exposition (SciTech)*, Kissimmee, FL, January 2015. doi:10.2514/6.2016-1294.

[12] Liem, R. P., Kenway, G. K. W., and Martins, J. R. R. A., "Multimission Aircraft Fuel Burn Minimization via Multipoint Aerostructural Optimization," *AIAA Journal*, Vol. 53, No. 1, January 2015, pp. 104–122. doi:10.2514/1.J052940.

[13] Hwang, J. T. and Martins, J. R. R. A., "Allocation-mission-design optimization of next-generation aircraft using a parallel computational framework," *57th AIAA/ASCE/AHS/ASC Structures, Structural Dynamics, and Materials Conference*, American Institute of Aeronautics and Astronautics, January 2016. doi:10.2514/6.2016-1662.

[14] Kota, S., Osborn, R., Ervin, G., Maric, D., Flick, P., and Paul, D., "Mission Adaptive Compliant Wing–Design, Fabrication and Flight Test," *RTO Applied Vehicle Technology Panel (AVT) Symposium*, 2009.

[15] Kao, J. Y., Hwang, J. T., Martins, J. R. R. A., Gray, J. S., and Moore, K. T., "A Modular Adjoint Approach to Aircraft Mission Analysis and Optimization," *Proceedings of the AIAA Science and Technology Forum and Exposition (SciTech)*, Kissimmee, FL, January 2015, AIAA 2015-0136.

[16] Jasa, J. P., Hwang, J. T., and Martins, J. R. R. A., "Open-source coupled aerostructural optimization using Python," *Structural and Multidisciplinary Optimization*, 2018, (Submitted).

[17] Heath, C. and Gray, J., "OpenMDAO: Framework for Flexible Multidisciplinary Design, Analysis and Optimization Methods," *Proceedings of the 53rd AIAA Structures, Structural Dynamics and Materials Conference*, Honolulu, HI, April 2012, AIAA-2012-1673.

[18] Hwang, J. T., *A modular approach to large-scale design optimization of aerospace systems*, Ph.D. thesis, University of Michigan, 2015.

[19] Martins, J. R. R. A. and Hwang, J. T., "Review and Unification of Methods for Computing Derivatives of Multidisciplinary Computational Models," *AIAA Journal*, Vol. 51, No. 11, November 2013, pp. 2582–2599. doi:10.2514/1.J052184.

[20] Reich, G. and Sanders, B., "Introduction to morphing aircraft research," *Journal of Aircraft*, Vol. 44, No. 4, 2007, pp. 1059–1059.

[21] Barbarino, S., Bilgen, O., Ajaj, R. M., Friswell, M. I., and Inman, D. J., "A review of morphing aircraft," *Journal of intelligent material systems and structures*, Vol. 22, No. 9, 2011, pp. 823–877.

[22] Sofla, A. Y. N., Meguid, S. A., Tan, K. T., and Yeo, W. K., "Shape Morphing of Aircraft Wing: Status and Challenges," *Materials & Design*, Vol. 31, No. 3, 3 2010, pp. 1284–1292. doi:10.1016/j.matdes.2009.09.011.

[23] Vos, R., Gürdal, Z., and Abdalla, M., "Mechanism for warp-controlled twist of a morphing wing," *Journal of Aircraft*, Vol. 47, No. 2, 2010, pp. 450.

[24] Hendricks, E. S., Falck, R. D., and Gray, J. S., "Simultaneous Propulsion System and Trajectory Optimization," *18th AIAA/ISSMO Multidisciplinary Analysis and Optimization Conference*, Denver, CO, June 2017.

[25] Falck, R. D., Chin, J. C., Schnulo, S. L., Burt, J. M., and Gray, J. S., "Trajectory Optimization of Electric Aircraft Subject to Subsystem Thermal Constraints," *18th AIAA/ISSMO Multidisciplinary Analysis and Optimization Conference*, Denver, CO, June 2017.

[26] Brooks, T. R., Kenway, G. K. W., and Martins, J. R. R. A., "uCRM: An Aerostructural Model for the Study of Flexible Transonic Aircraft Wings," *AIAA Journal*, (Submitted).

[27] Vassberg, J. C., DeHaan, M. A., Rivers, S. M., and Wahls, R. A., "Development of a Common Research Model for Applied CFD Validation Studies," 2008, AIAA 2008-6919.

[28] Vassberg, J. C., Tinoco, E. N., Mani, M., Rider, B., Zickuhr, T., Levy, D. W., Brodersen, O. P., Eisfeld, B., Crippa, S., Wahls, R. A., Morrison, J. H., Mavriplis, D. J., and Murayama, M., "Summary of the Fourth AIAA Computational Fluid Dynamics Drag Prediction Workshop," *Journal of Aircraft*, Vol. 51, No. 4, jul 2014, pp. 1070–1089. doi:10.2514/1.c032418.

[29] Hwang, J. T. and Munster, D. W., "Solution of ordinary differential equations in gradient-basedmultidisciplinary design optimization," *2018 AIAA/ASCE/AHS/ASC Structures, Structural Dynamics, and Materials Conference*, Orlando, FL, January 2018.

[30] Hwang, J. T. and Martins, J. R. R. A., "A fast-prediction surrogate model for large datasets," *Aerospace Science and Technology*, 2017.

[31] Claus, R. W., Evans, A. L., and Follen, G. J., "Multidisciplinary propulsion simulation using NPSS," *AIAA Paper*, Vol. 92, 1992, pp. 4709.

[32] Gill, P. E., Murray, W., and Saunders, M. A., "SNOPT: An SQP Algorithm for Large-Scale Constrained Optimization," *SIAM Review*, Vol. 47, No. 1, 2005, pp. 99–131. doi:10.1137/S0036144504446096.

[33] Kreisselmeier, G. and Steinhauser, R., "Systematic Control Design by Optimizing a Vector Performance Index," *International Federation of Active Controls Symposium on Computer-Aided Design of Control Systems, Zurich, Switzerland*, 1979.